Available online at www.sciencedirect.com
SciVerse ScienceDirect
Journal of the European Ceramic Society 32 (2012) 1821–1835
www.elsevier.com/locate/jeurceramsoc

Preparation and properties of B_6O/TiB_2-composites

Maik Thiele [a,*], Mathias Herrmann [a,c], Jan Räthel [a,d], Hans-Joachim Kleebe [b,e], Mathis Manfred Mueller [b,f], Tim Gestrich [a,g], Alexander Michaelis [a,h]

[a] *Fraunhofer-Institute of Ceramic Technologies and Systems, Winterbergstraße 28, 01277 Dresden, Germany*
[b] *Institute for Applied Geosciences, FG Geomaterial Science, Schnittspahnstraße. 9, 64287 Darmstadt, Germany*

Received 6 November 2011; received in revised form 14 December 2011; accepted 15 December 2011
Available online 25 January 2012

Abstract

B_6O/TiB_2 composites with varying compositions were produced by FAST/SPS at temperatures between 1850 and 1900 °C following a non-reactive or a reactive sintering route. The densification, phase and microstructure formation and the mechanical and thermal properties were investigated. The comparison to an also investigated pure B_6O material showed that the addition of TiB_2 in a non-reactive sintering route promotes the B_6O densification. Further improvement was obtained by sintering reactive B–TiO_2 mixtures which also results in materials with a finer grain size and thus in enhanced mechanical properties. The fracture toughness was significantly improved in all composites and is up to 4.0 MPa m$^{1/2}$ (SEVNB) and 2.6–5.0 MPa m$^{1/2}$ (IF method) while simultaneously a high hardness of up to 36 GPa ($HV_{0.4}$) and 28 GPa (HV_5) could be preserved. The high temperature properties at 1000 °C of hardness, thermal conductivity and CTE were up to 20 GPa, 18 W/mK and 6.63×10^{-6}/K, respectively.

Keywords: Boron suboxide; Mechanical properties; Thermal properties; Microstructure-final; Wear parts

1. Introduction

Boron suboxide (B_6O) is known to possess excellent mechanical properties with a reported average hardness of 45 GPa and a fracture toughness of 4.5 MPa m$^{1/2}$ measured on single crystals.[1] Thus it is often regarded as a promising candidate for applications with a high demand in wear resistance and as an alternative for diamond and cubic boron nitride (c-BN) based materials. Although boron suboxide can be economically synthesized near ambient pressures[2–5] its commercial use is actually prevented by its poor sinterability due to low diffusion coefficients and a high vapor pressure beside a resulting low fracture toughness of polycrystalline B_6O materials. Full densification of B_6O materials usually requires high pressures (1–5 GPa) but the resulting fracture toughness will not exceed 2 MPa m$^{1/2}$.[6–8] Also efforts to improve the fracture toughness by the preparation of composites with other hard materials such as diamond,[9] boron carbide[10] or c-BN[11] only result in materials with very high hardness up to 46 GPa but a fracture toughness lower than 1.8 MPa m$^{1/2}$. Full densification can alternatively achieved by hot pressing reactive mixtures of B and B_2O_3 at temperatures up to 2000 °C.[12,13] Although this will results in materials with a high microhardness no further mechanical properties were reported.

Actual research is focusing on the use of oxide additives or metals which form a liquid phase during sintering and thus allow the reproducible production of full densified B_6O materials by low pressure sintering techniques like hot pressing or field assisted sintering technology/spark plasma sintering (FAST/SPS).[14–21] These materials are reported to exhibit an increased fracture toughness of about 3–4 MPa m$^{1/2}$ while the hardness is only marginally lowered.

In this study the preparation and the microstructural, mechanical and thermal properties of B_6O/TiB_2 composites

* Corresponding author. Tel.: +49 351 2553 7546.
E-mail addresses: Maik.Thiele@ikts.fraunhofer.de (M. Thiele), Mathias.Hermann@ikts.fraunhofer.de (M. Herrmann), jan.raethel@ikts.fraunhofer.de (J. Räthel), Kleebe@geo.tu-darmstadt.de (H.-J. Kleebe), mueller@geo.tu-darmstadt.de (M.M. Mueller), tim.gestrich@ikts.fraunhofer.de (T. Gestrich), alexander.michaelis@ikts.fraunhofer.de (A. Michaelis).
[c] Tel.: +49 351 2553 7527; fax: +49 351 2554 122.
[d] Tel.: +49 351 2553 7967.
[e] Tel.: +49 6151 16 4554; fax: +49 6151 16 4021.
[f] Tel.: +49 6151 16 2180.
[g] Tel.: +49 351 2553 7814.
[h] Tel.: +49 351 2553 7512; fax: +49 351 2554 300.

0955-2219/$ – see front matter © 2012 Elsevier Ltd. All rights reserved.
doi:10.1016/j.jeurceramsoc.2011.12.034

are investigated. Since titanium diboride is itself characterized by a high hardness (25 GPa, HV_5), a good thermal conductivity (96 W/mK), a low density (4.5 g/cm^3) and a good chemical stability[22] it can be expected that the formation of B_6O/TiB_2 composites may result in materials with enhanced performance for structural and wear applications. This was already indicated by Herrmann et al. who reported a considerable microhardness of 37 GPa ($HV_{0.4}$) for a B_6O composite containing 10 wt.% TiB_2 and 4 wt.% oxide additives densified by FAST/SPS.[14] Furthermore this work demonstrated that the application of a reactive sintering route on the basis of mixtures of TiH_2–B_6O or B–TiO_2 is an alternative and cost-effective method for the composite preparation. However, beside a hardness of 34 GPa for the B_6O–TiH_2 reactive route no further properties were reported. Therefore the aim of this work is a more detailed view and a systematic investigation of the properties of FAST/SPS densified B_6O/TiB_2 composites resulting from different preparation routes and starting compositions. A main aspect would be to point out whether the incorporation of TiB_2 in a matrix of B_6O can improve the fracture resistance and therefore minimizing or eliminating one of the major shortcomings of B_6O materials. Moreover the phase formation and the microstructure development during reactive sintering of B–TiO_2 mixtures will be discussed.

2. Experimental and analytical methods

2.1. Experimental techniques

Two different procedures were used for producing B_6O/TiB_2 composite materials: a non-reactive and a reactive sintering route. A complete overview of all produced compositions is given in Table 1.

2.1.1. Non-reactive materials

Materials of the non-reactive route were prepared by sintering admixed powders of B_6O and TiB_2 (Grade F, ABCR GmbH, Germany) with varying B_6O/TiB_2 ratios between 0.8 and 15.2 (56.9–6.2 vol.%; Table 1). The used boron suboxide powder was fabricated by reducing boron oxide (Merck, Germany) with amorphous boron (Grade I, H.C. Starck, Germany) in a furnace with tungsten heaters (FSW 315/400-1600-NE, FCT, Germany) at 1300 °C for 6 h under flowing argon atmosphere according to methods reported in literature.[8–11,20] The resulting product was milled in several steps using a jaw crusher and a jet mill and afterwards was washed in ethanol to remove residual B_2O_3 remaining from the synthesis. The average grain size (d_{50}) of the final B_6O powder was 2.04 μm as determined by Mastersizer 2000 (Malvern Instruments Ltd, UK). Chemical analysis by Inductively Coupled Plasma Optical Emission Spectrometry (ICP-OES, iCAP 6000, Thermo Scientific, USA) identified minor impurities of Mg (0.37%), Al (0.14%) and Fe (0.11%) which were introduced through the starting materials as well as the powder processing procedure.

2.1.2. Reactive materials

In the reactive route premixed powders of amorphous boron (Grade I, H.C. Starck, Germany) and TiO_2 (P25, Degussa, Germany) are converted to B_6O and TiB_2 during heat treatment according to the equation:

$$14B + TiO_2 = 2B_6O + TiB_2 \quad (1)$$

Assuming the formation of stoichiometric B_6O with a density of 2.55 g/cm^3 this reaction will result in a B_6O/TiB_2 composite material with a calculated composition of 80.5 vol.% B_6O and 19.5 vol.% TiB_2. In order to increase the B_6O/TiB_2 ratio of the final product, pre-milled B_6O was partially added to the starting compositions. The overall B_6O/TiB_2 ratio of the reactive composition was between 4.1 and 8.1 (19.5–11 vol.%; Table 1). Furthermore to some of the reactive mixtures additional boron in a quantity between 12.1 and 12.5 wt.% was added to investigate the influence of a reduced oxygen stoichiometry on the phase formation.

Beside the pure compositions consisting only of B_6O and TiB_2, some non-reactive as well as reactive powder compositions were blended with additional oxide sintering additives. A total amount of 4.4–4.8 wt.% Al_2O_3 (AKP 50, Sumitomo Chemical, Japan) and Y_2O_3 (Grade C, H.C. Starck, Germany) with a molar ratio $Al_2O_3/(Al_2O_3 + Y_2O_3)$ of approximately 62.5 were added.

All batches were mixed in a laboratory attrition mill (PE075, Netzsch, Germany) with ethanol as a solvent. During this process the average grain size of starting materials is further reduced. In the case of compositions without addition of oxide additives tungsten carbide milling balls (Ø 1.57 mm; WC10Co) were used. Otherwise mixing was performed using alumina milling balls (Ø 1–2 mm, 99.6% purity). Milling time was 2 h for reactive compositions and 6 h for non-reactive composition with TiB_2 content < 20 vol.%. Compositions with TiB_2 > 20 vol.% were processed for 2 h. After milling the suspension was dried using a rotavap and granulated on a sieve with a mesh size of 400 μm. The wear of the milling balls was included in the calculation of the overall composition.

2.1.3. Sintering

Sintering of the non-reactive and reactive powder mixtures was carried out in a FAST/SPS furnace (HP D25, FCT, Germany) by using graphite dies of 30–60 mm in diameter and graphite foils coated with hBN in order to inhibit chemical reaction with the sample material. Since the hBN coating is electrical non-conductive direct current flow through the sample volume is prevented. Therefore the sintering process is rather more related to a fast hot pressing than a FAST/SPS. Sintering temperature was 1850 °C or 1900 °C and controlled by a pyrometer in the centre of the punch. A total load of 50 MPa was applied at a temperature between 900 and 1000 °C. The heating rate was 50 K/min, the dwell time at maximum temperature was 5 min and sintering atmosphere was argon or vacuum. The densification was recorded by measurement of the displacement which also includes small contributions from thermal expansion of the used system. These contributions can

Table 1
List of investigated samples including composition, sintering temperature, density and resulting phases after densification (XRD, SEM, TEM). Sample declaration: "r", reactive sintered; "nr", non-reactive sintered; "a", oxide additives used; "e", reduced oxygen stoichiometry/excess boron.

Sample	Composition			Additives			Density (g/cm^3)	Sintering temperature (°C)	Phases after sintering
	B_6O (vol.%)	TiB_2 (vol.%)	$TiB_2/(TiB_2 + B_6O)$ vol. ratio	B^{excess} (wt.%)	Oxide Add. (wt.%)	WC[a] (wt.%)			
Pure B_6O									
Pure	100	–	–	–	–	–	2.52	1900	B_6O
Non-reactive sintered materials									
nr-1	80.4	19.6	0.20	–	–	5.6	2.98	1850	B_6O; TiB_2; $(Ti,W)B_2$
nr-2	63.9	36.1	0.36	–	–	4.6	3.21	1850	B_6O; TiB_2; $(Ti,W)B_2$
nr-3	43.1	56.9	0.57	–	–	3.5	3.61	1850	B_6O; TiB_2; $(Ti,W)B_2$
nr-4a	80.5	19.5	0.20	–	4.7	–	2.90	1900	B_6O; TiB_2; amorph. phase
nr-5a	93.8	6.2	0.06	–	4.8	–	2.70	1850	B_6O; TiB_2; amorph. phase
Reactive sintered materials (B_6O; TiB_2 calculated after reaction $TiO_2 + 14B = TiB_2 + 2B_6O$)									
r-1	80.5	19.5	0.20	–	–	1.6	2.89	1850	B_6O; TiB_2
r-2e	80.5	19.5	0.20	12.1	–	1.5	2.99	1900	B_6O; TiB_2; B
r-3a	80.5	19.5	0.20	–	4.7	–	2.91	1850	B_6O; TiB_2; amorph. phase
r-4a	89.0	11.0	0.11	–	4.4	–	2.75	1850	B_6O; TiB_2; amorph. phase
r-5ae	80.5	19.5	0.20	12.5	4.7	–	2.84	1850	B_6O; TiB_2; B; amorph. phase

[a] Introduced by milling ball abrasion.

be eliminated by subtracting the recorded piston travel during an adjacent sintering run with identical setup including the previously fully densified sample. This was exemplary done for some materials. The correlation of the measured final density with the piston travel at the end of the dwell time then allows the calculation of relative densities as function of sintering temperature and sintering time. Beside the standard sintering procedure FAST/SPS sintering runs for a reactive mixture were terminated at specified temperatures (750 °C, 820 °C, 1380 °C, 1410 °C and 1470 °C) in order to determine the evolution of different species and phase composition as a function of sintering temperature.

Additionally, a pure B_6O material was produced as reference material. For this purpose the prepared B_6O powder was milled for 4 h in a laboratory batch mill using steel balls (Ø 2.5 mm) and ethanol as solvent. The milling ball abrasion was removed by washing the powder several times in HCl. Densification was carried out using FAST/SPS at sintering temperature of 1900 °C and other parameters comparable to that of the produced B_6O/TiB_2 materials.

2.2. Analytical methods

2.2.1. Phases and microstructure

After consolidation density and open porosity of the materials were measured by Archimedes method and compared with theoretical densities, which were estimated using the rule of mixture. Afterwards all samples were cut and qualitative phase analysis was performed by X-Ray Diffraction (XRD, XRD7, GE Inspection) using CuKa radiation.

Mechanical polished cross-sections of all materials were investigated by Field Emission Scanning Electron Microscopy (FESEM, ULTRA 55, CARL ZEISS, Germany) with an Energy Dispersive X-ray Spectroscopy (EDS) system attached to it. The average grain size (d_{50}) of phases was exemplary determined by linear analysis of SEM micrographs. In order to visualize the B_6O grain boundaries high contrast images were taken with the In-lens SE detector at a magnification of 20kx for the non-reactive materials and 25kx for reactive sintered compositions. As suggested for non-textured, polycrystalline materials the measured intercept lengths were afterwards corrected by a factor of 1.56.[23]

For some samples Transmission Electron Microscopy (TEM) was carried out with a Philips CM20 microscope (FEI, Eindhoven, the Netherlands; equipped with a LaB_6 cathode and a JEM 2100F (Jeol, Tokyo, Japan) equipped with a Schottky FEG, both using a nominal acceleration voltage of 200 kV. Chemical Analysis was performed with a TEM 250 EDS detector (Oxford, Wiesbaden, Germany) attached to the JEM 2100F. TEM samples were prepared using standard ceramographic techniques, which included grinding, dimpling, and ion milling, followed by coating the sample with a thin carbon layer to avoid charging of the sample under the incident electron beam.

In order to understand the phase formation during the consolidation of reactive compositions thermogravimetric (TG) and differential thermal analysis (DTA) were carried out using a STA 449C synchronous thermal analyzer (NETZSCH, Germany) at a temperature up to 1500 °C. The investigated reactive mixture was composed of 64.4 wt.% boron, 34.9 wt.% TiO_2 and 1.7 wt.% WC (sample r-1). The heating rate was 10 K/min and atmosphere was argon. Together with the collected XRD data from the aborted sintering runs this investigation serves the stepwise reconstruction of the reaction path during sintering.

2.2.2. Mechanical properties

For microhardness ($HV_{0.4}$) and macrohardness (HV_5) testing a MHT-10 apparatus with Vickers indenter (Anton Paar, Austria) and AVK 50 (Akashi, Japan) was used. The indentations were done on mechanical polished surfaces with a load of 3.9 N ($HV_{0.4}$) and 49 N (HV_5), respectively. The load was kept constant at highest load for 10 s ($HV_{0.4}$) or 15 s (HV_5). The high temperature hardness was determined in an apparatus developed together with Hegewald & Peschke (Germany) which can measure the hardness up to 1500 °C in vacuum. Indentions at a total load of 49 N (HV_5) were done up to 1000 °C. The indentation was held at the highest load for 10 s. For all hardness investigations average hardness and standard deviation were calculated on the basis of the measurement of 5 indentations by optical microscopy.

The cracks originating from hardness testing at 49 N (HV_5) were used to calculate fracture toughness by the indention fracture (IF) method on the basis of the equitation given by Anstis (E = 480 GPa).[24] Relative error of resulting K_IC values can be estimated to be 15–20%. Additionally for some materials more reliable values of fracture toughness were determined by Single Edge V-notch Beam (SEVNB) technique. Therefore V-notched bending bars (notch radius 20–30 μm) with a dimension of 3 mm × 4 mm × 45 mm were prepared and tested by the 4-point-bending technique (40/20 mm span of the supports). Fracture toughness was then calculated in accordance to ISO 23146:2008.

2.2.3. *Thermal properties*

For exemplary compositions thermal conductivity as function of temperature λ(T) was calculated on the basis of measured values for thermal diffusivity, density (corrected by thermal expansion measurement) and specific heat. Therefore thermal diffusivity as function of temperature $a(T)$ was measured up to 1000 °C by Laser Flash method (LFA) using LFA 427 (NETZSCH, Germany). The thermal expansion $\alpha(T)$ was derived from dilatometric analysis using a DIL402 dilatometer (NETZSCH, Germany) with a heating rate of 2 K/min up to 1000 °C within a relative error of 5%. Measurement of specific heat $c_P(T)$ between RT and 1000 °C was only done for pure B_6O material using differential scanning calorimetry DSC404 (NETZSCH, Germany). Specific heat for other materials was then approximated by the rule of mixture using additional literature data for specific heat of TiB_2[26] and the calculated volume content of B_6O and TiB_2 in the final material. Total error of the resulting calculated thermal conductivity can be approximated to be 15%. Because of the higher uncertainty of measurements of specific heat and thermal diffusivity at low temperatures direct measurement of thermal conductivity near room temperature were additionally carried out using a TCT 416 (NETZSCH, Germany) to verify the calculated values. This was exemplary done for the pure B_6O material and one non-reactive sintered sample (sample nr-1). Measurement temperature was 48 °C, the relative Error of the derived values is 5%.

3. Results

3.1. *Densification and phase formation*

Depending on the sample composition the resulting densities of the sintered composites are between 2.70 g/cm^3 (sample nr-5ae) and 3.61 g/cm^3 (sample nr-3a) for the non-reactive samples and in the range of 2.75 g/cm^3 (sample r-4a) and 2.99 g/cm^3 (sample r-2e) for the reactive sintered materials, respectively (Table 1). For all samples only minor amounts of open porosity between 0.1 vol.% and 0.8 vol.% are measured by Archimedes method. Based on SEM micrographs, which show nearly no porosity, it can be therefore concluded that all reported non-reactive as well as reactive sintered B_6O/TiB_2 composites are fully densified at temperatures between 1850 °C and 1900 °C. Minor but significant porosity is only observed for WC milled non-reactive densified materials, which may be at least partially connected with TiB_2 phase pullout during mechanical polishing.

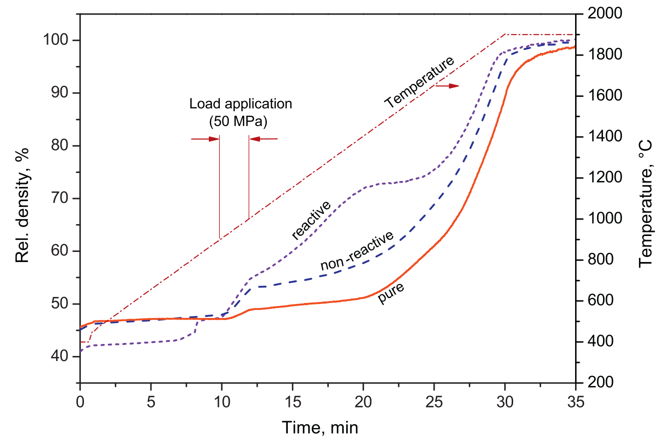

Fig. 1. Exemplary FAST/SPS densification curves (thermal expansion of sintering equipment corrected) of a non-reactive and a reactive sintered B_6O/TiB_2 composite with additional Al_2O_3/Y_2O_3 additives (sample composition r-3a; nr-4a). For comparison the sintering curve of a pure B_6O material is illustrated.

Exemplary FAST/SPS densification curves of a non-reactive and a reactive sintered material containing 19.5 vol.% TiB_2 and 4.7 wt.% Al_2O_3/Y_2O_3 additives, respectively (composition r-3a; nr-4a) are depicted in Fig. 1. Additionally the sintering curve of a pure B_6O material without additives is illustrated.

3.1.1. *Non-reactive materials*

In comparison to the pure B_6O powder the addition of TiB_2 and oxide additives in the non-reactive material significantly increases the resulting density after the load application between 900 and 1000 °C and decreases the onset temperature for sintering to 1300–1350 °C. Thus a higher relative density at the beginning of the dwell time of about 97% is achieved and only minor densification takes place during the dwelling time itself. All compositions were fully densified after sintering. Phase analysis by XRD shows a final composition of B_6O beside TiB_2 for all compositions (Table 1). Peaks connected with a possible formation of crystalline Al–Y–O phases in the materials with oxide additives (samples nr-4a; nr-5a) are not observed. Furthermore, and despite of partially high abrasion of WC (3.5–5.6 wt.%) in the case of powder preparation by milling with WC-balls, no formation of separate, crystalline tungsten containing phases were found by XRD.

3.1.2. *Reactive materials*

The recorded densification curve for the reactive sintered composition in figure 1 differs significantly from that of the non-reactive compositions. The densification is characterized by a first strong densification between 750 °C and 820 °C. In situ measurement of the electric current during FAST/SPS show a

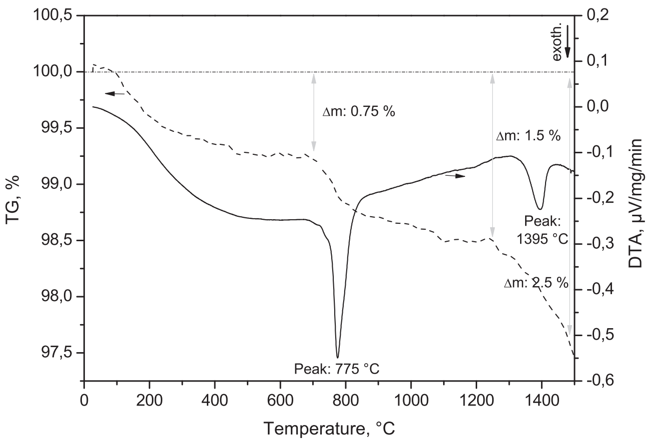

Fig. 2. DTA/TG curves of a reactive mixture consisting of 64.4 wt.% boron, 34.9 wt.% TiO_2 and 1.7 wt.% WC (sample composition r-1) for a temperature up to 1500 °C.

temporary erratic drop of the heating power in this temperature range and is therefore indicating the occurrence of a strong exothermic reaction. This is confirmed by DTA/TGA analysis which was performed on a stoichiometric reactive mixture (sample r-1) and is illustrated in Fig. 2. It is shown that up to approximately 500 °C the powder mixture is characterized by a decrease in mass of about 0.75 wt.% which is also accompanied by a slight but significant exothermic reaction. The observed strong exothermic reaction then starts at about 700 °C, ends at about 830 °C and has its peak temperature at about 775 °C. During the reaction a reduction in mass of about 0.5 wt.% is measured. The results of XRD analysis of the terminated FAST/SPS runs before and after this first reaction are depicted in Fig. 3. The data reveals that TiB_2 is formed from an initial mixture at 750 °C consisting of a non-altered phase TiO_2 (anatase modification), boron (predominantly amorphous), a chemical reduced compound TiO_{2-x} (Ti_3O_5, Ti_4O_7 could be assigned) as well as $TiBO_3$. After the reaction the material is composed only of TiB_2 with relative low crystallinity beside boron and no further densification is observed up to 900 °C. Thus, all oxide phases have disappeared. Significant further densification then again starts at a temperature between 900 and 1000 °C and notably reduces at a temperature of 1450 °C (Fig. 1). The exact onset of the sintering is overlaid by the application of mechanical load. A second exothermic reaction with lower intensity, also characterized by a small drop of heating power during FAST/SPS processing, is observed in that temperature range at a temperature of about 1400 °C. By DTA/TGA measurements (Fig. 2) a peak temperature of about 1395 °C could be assigned to this reaction while XRD results (Fig. 3) indicate the formation of B_6O on the cost of remaining boron which is disappearing in XRD data. Further slight reduction in mass takes place during this process. Afterwards densification is stagnating until the third major densification phase starts at about 1650 °C resulting in a relative density of 98–99% at the beginning of the dwelling time, thus slightly exceeding that of the non-reactive sintered material. During the last densification step crystallinity of B_6O and TiB_2 is further increased as indicated by the decreasing Full Width at Half Maximum (FWHM) of the taken XRD pattern. Full densification was obtained at the end of the dwell time. Phase analysis by XRD shows a final composition of B_6O beside TiB_2 for all investigated reactive sintered compositions listed in Table 1. In materials with oxygen deficiency (sample r-2e; r-5ae) generally a lower crystallinity of the B_6O phase is observed. Furthermore the diffraction pattern of these samples

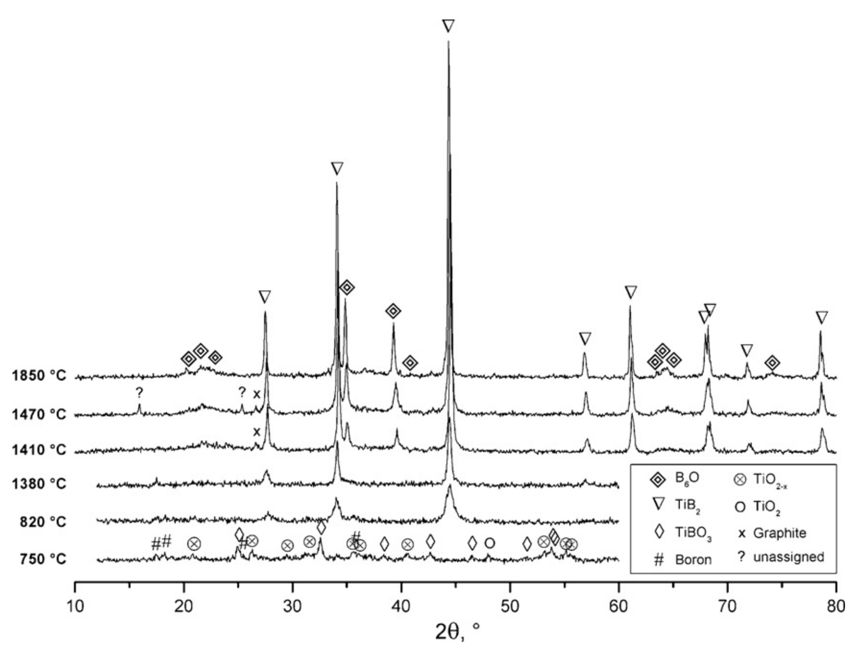

Fig. 3. Comparison of XRD data showing phase composition at different sintering temperature of a reactive sintered mixture consisting of 64.4 wt.% boron, 34.9 wt.% TiO_2 and 1.7 wt.% WC (sample composition r-1). Except of the pattern for 1850 °C all pattern are measured on aborted FAST/SPS runs without dwelling time. At 1470 °C two unassigned peaks are marked by "?". The peak marked with "X" may be related to graphite from the FAST/SPS tool setup.

Table 2
Results of linear analysis on SEM micrographs for a non-reactive (sample nr-4a) and a reactive (sample r-3a) B_6O/TiB_2 composite with similar composition. Additionally results for a pure material are listed.

Phase	Counts	d_{10} (nm)	d_{50} (nm)	d_{90} (nm)
Pure B_6O material				
B_6O	967	89	276	704
Pores	40	45	89	294
Non-reactive sintered material (sample nr-4a)				
B_6O	1611	80	223	508
TiB_2	154	205	642	1471
Amorph. phase	452	36	107	330
Reactive sintered material (sample r-3a)				
B_6O	1615	71	163	319
TiB_2	262	99	262	468
Amorph. phase	363	28	85	269

indicates the additional presence of some non-reacted boron after densification. In accordance to the results for the non-reactive preparation route no additional crystalline Al–Y–O phases could be assigned in the XRD data for the reactive sintered compositions with oxide additives (samples r-3a, r-4a, r-5ae).

3.2. Microstructure

3.2.1. Non-reactive materials

Exemplary SEM micrographs of the non-reactive sintered materials with composition of 19.5 vol.% TiB_2 and oxide additives (sample nr-4a) are illustrated in Fig. 4a and b. The microstructure is characterized by homogeneously distributed TiB_2 grains in a matrix of B_6O. Additionally a secondary phase with a composition of Al–Y–O–B as determined by EDS measurements is present in the triple junctions in all materials which are composed of additional oxide additives. As already indicated by XRD analysis, electron diffraction performed during TEM investigations show that this phase is amorphous and not wets the interface between adjacent B_6O grains as well as between B_6O and TiB_2 particles. Generally a high density of stacking faults and dislocations are present in the B_6O grains. Table 2 list results for the grain size distribution as derived by linear analysis. The average grain size d_{50} is about 220 nm for B_6O, 640 nm for TiB_2 and approximately 110 nm for the amorphous phase. In comparison to the pure B_6O material the B_6O grain size is therefore slightly smaller and characterized by a narrower grain size distribution. TiB_2 grains are of irregular shape und show a wide grain size distribution with a measured grain size within a range of 50 nm up to 2.2 μm. The measured TiB_2 phase content of about 19 vol.% in sample nr-4a is in agreement to the starting composition.

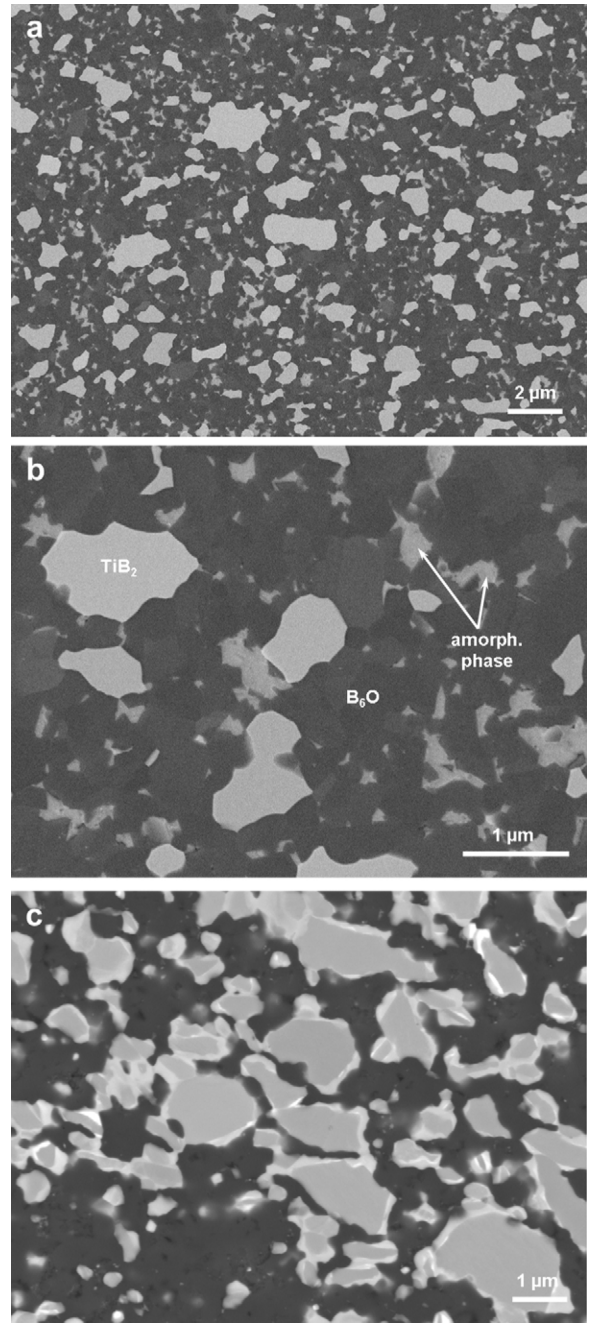

Fig. 4. SEM micrographs of non-reactive sintered materials. (a) SE-image of sample nr-4a showing homogenously distributed TiB_2 (light grey) and an amorphous phase (grey) with irregular shape in a matrix of B_6O (dark). (b) Higher magnification of the same sample with labeled phases. (c) BSE-image of sample nr-2 showing $(Ti,W)B_2$ rim (bright) on TiB_2 grains (grey) in a matrix of B_6O (dark).

As depicted in Fig. 4c the formation of a core-rim structure in TiB_2 grains is observed for samples prepared by WC milling and densification without oxide additives (samples nr-1; nr-2; nr-3). Fig. 5 illustrates TEM investigations performed on these grains in sample nr-1. EDS analysis and electron diffraction show that the core is composed of TiB_2 with space group P6/mmm while the rim is of the same crystal structure and formed by a solid solution with composition of $(Ti,W)B_2$ and minor amounts of aluminum. TEM investigations furthermore reveal the presence of finely distributed micropores with diameter below 50 nm in this sample. These may be at least partially a preparation artifact through strong tendency of TiB_2 grain pullout during mechanical polishing in non-reactive sintered samples without oxide additives. However, no clear indication of insufficient

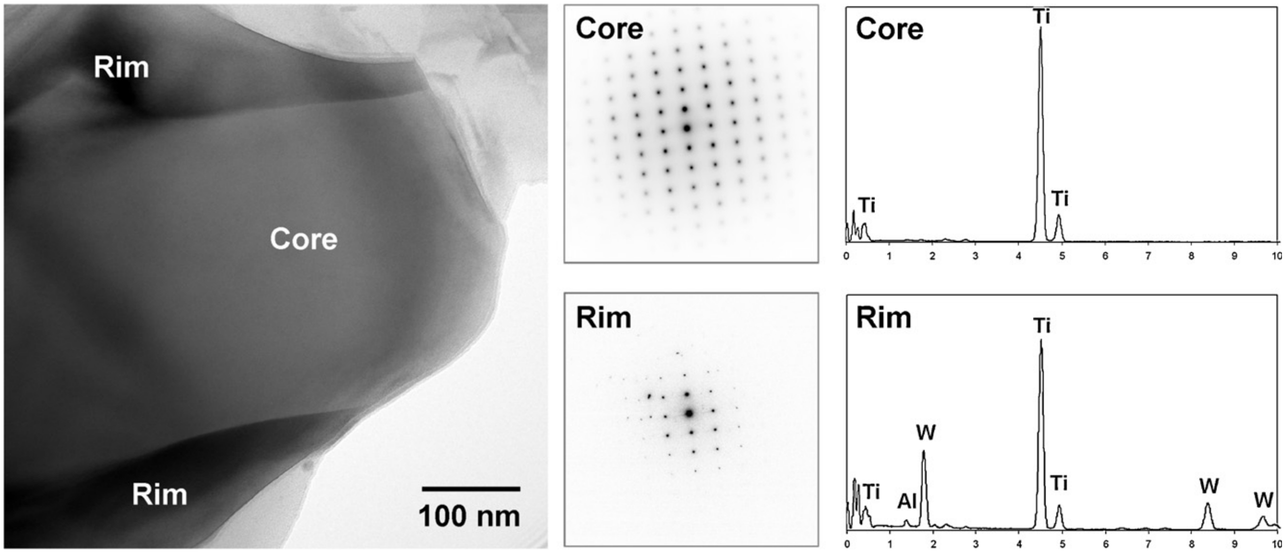

Fig. 5. TEM image depicting a TiB_2 grain with core-rim structure in the non-reactive sintered sample nr-1. EDS and electron diffraction results of the outer rim and the core are illustrated, respectively, revealing chemical zoning and an identical crystal structure.

binding between B_6O and TiB_2 grains was found in TEM investigations.

3.2.2. Reactive materials

The observed phase composition of reactive sintered B_6O/TiB_2 composites is generally similar to that of non-reactive sintered materials with occurrence of B_6O beside TiB_2 and the formation of an amorphous Al–Y–O–B containing phase in the case of oxide additives used. In Fig. 6a and b SEM micrographs of the material with a calculated composition of 19.5 vol.% TiB_2 and oxide additives (sample r-3a) are depicted. Comparing the microstructure with that of the non-reactive sample with similar composition and taken at same magnification (Fig. 4a and b) it is obvious that the reactive-sintering route results in B_6O/TiB_2 composites with a much finer average grain size and a narrower grain size distribution for all formed phases. As listed in Table 2 the average grain size d_{50} is about 160 nm for B_6O, 260 nm for TiB_2 and approximately 80 nm for the Al–Y–O–B containing amorphous phase. The addition of prereacted B_6O in order to increase the B_6O/TiB_2 ratio in sample r-4a results in slightly larger average B_6O grain size. The measured TiB_2 volume content of about 19 vol.% of sample r-3a fits well with the calculated composition. In contrast to the non-reactive sintered compositions TiB_2 grains are often clearly facetted and hexagonal symmetry can be observed. Electron beam diffraction indicates good crystallinity of the formed TiB_2 phase. Contrary B_6O grains often show dislocations and stacking faults but generally in a lesser extent than in non-reactive materials. Fig. 6c shows a typical TEM micrograph of sample nr-5ae with 19.5 vol.% TiB_2, oxide additives and reduced oxygen stoichiometry. Within the amorphous secondary phase the formation of phase separations (bright circular regions) of approximately 10 nm in diameters are observed but could not be chemically analyzed by EDS due to immediate phase damage as the amorphous phase is beam sensitive. Generally in the materials with boron in excess (samples r-2e; r-5ae) unreacted boron is found in microstructure investigations, especially if oxide additives are used (sample r-5ae).

3.3. Properties

3.3.1. Hardness and fracture toughness

The results of macrohardness (HV_5), microhardness ($HV_{0.4}$) and fracture toughness measurements by IF and SEVNB method are listed in Table 3.

For non-reactive compositions a hardness value between 15.3 GPa (sample nr-3) and 23.5 GPa (sample nr-5a) and a microhardness in the range of 26.6 GPa (sample nr-3) and 31.3 GPa (sample nr-1) were obtained. The hardness of reactive sintered materials is generally higher than that of non-reactive compositions. The macrohardness is in the range of 21.6 GPa (sample r-4a) and 27.9 GPa (sample r-2e) while the derived microhardness is between 28.8 GPa (sample r-1) and 35.6 GPa (sample r-4a). Thus the hardness of some reactive sintered materials is close to that of the pure B_6O material.

In comparison to the pure B_6O material the fracture toughness is significantly increased for all reported non-reactive and reactive produced B_6O/TiB_2 composites. The fracture toughness obtained by the IF method for the non-reactive sintered materials is between 2.8 MPa $m^{1/2}$ (sample nr-5a) and 5.0 MPa $m^{1/2}$ (sample nr-3), while the highest values of 4.7–5.0 MPa $m^{1/2}$ are measured for the materials with the highest amount of TiB_2. Fracture toughness obtained through SEVNB technique generally exceeds that of corresponding values derived from IF method. For the non-reactive sintered materials values of 3.1 MPa $m^{1/2}$ (sample nr-5a) and 4.0 MPa $m^{1/2}$ (sample nr-1) are measured in SEVNB tests. The reactive sintered composition are characterized by a fracture toughness (IF method) in the range of 2.6 MPa $m^{1/2}$ (sample r-2e) and 3.0 MPa $m^{1/2}$ (sample r-1; r-3a). In respect to an estimated relative error of

Table 3
Hardness at different loads and temperatures beside the fracture toughness obtained by IF and SEVNB method. Measurement of the fracture toughness of pure B_6O was not possible by IF method because of chipping at the used load of 49 N. "RT"–Room temperature.

Sample	Hardness (GPa)					K_IC (MPa m$^{1/2}$)	
	$HV_{0.4}$	HV_5 (RT)	HV_5 (600 °C)	HV_5 (800 °C)	HV_5 (1000 °C)	IF method	SEVNB
Pure B_6O material							
Pure	35–37	24–28	22.4 ± 0.8	21.1 ± 0.6	20.7 ± 0.4	Brittle	2.0 ± 0.4
Non-reactive sintered materials							
nr-1	31.3 ± 0.5	21.8 ± 0.8	–	14.0 ± 0.4	12.8 ± 0.2	2.9	4.0 ± 0.5
nr-2	27.5 ± 1.4	18.0 ± 1.0	–	–	–	4.7	–
nr-3	26.6 ± 1.4	15.3 ± 0.5	–	–	–	5.0	–
nr-4a	30.4 ± 0.9	22.7 ± 1.0	–	–	–	2.9	–
nr-5a	29.0 ± 0.9	23.5 ± 0.4	–	18.7 ± 0.2	19.6 ± 0.3	2.8	3.1 ± 0.4
Reactive sintered materials							
r-1	28.8 ± 0.5	22.6 ± 0.4	–	16.1 ± 0.3	15.1 ± 0.6	3.0	–
r-2e	32.1 ± 0.9	27.9 ± 2.5	–	–	–	2.6	3.6 ± 0.2
r-3a	35.5 ± 0.8	23.1 ± 0.5	–	–	–	3.0	–
r-4a	35.6 ± 0.7	21.6 ± 0.5	–	–	–	2.8	–
r-5ae	32.6 ± 0.9	24.1 ± 0.7	–	–	–	2.9	–

15–20% for the IF method these values do not indicate a significant difference between the different preparation routes. In SEVNB measurement a value of 3.6 MPa m$^{1/2}$ for sample r-2e was obtained.

3.3.2. High temperature hardness

The results of the hardness measurement (HV_5) as function of temperature up to 1000 °C are given in Table 3 and illustrated in Fig. 7. Generally all investigated B_6O/TiB_2 composites are characterized by a nearly linear decrease of hardness with rising temperature. In contrast the pure B_6O material shows the tendency of non-linear dependence with higher reduction of hardness as function of temperature lower than 600 °C. In the whole temperature range the hardness of all composites is below that of the pure reference material. Since the reactive composition (sample r-1) are characterized by a superior high temperature hardness in comparison to its non-reactive counterpart with similar composition (sample nr-1) and the non-reactive material with lowest total TiB_2 content (sample nr-5a) shows the highest high temperature hardness of all composites, the results are in agreement with the conventional hardness measurements at room temperature. The total reduction of hardness up to 1000 °C is highest for the non-reactive material with 19.6 vol.% TiB_2 (sample nr-1) and about 33%. For all other measured compositions, including the pure material, a lower average decrease of hardness with increasing temperature of about 25% is observed.

3.3.3. Thermal properties

Figs. 8 and 9 present the results of the measurement of thermal diffusivity for different B_6O/TiB_2 composites in comparison to a pure B_6O material and the specific heat for the pure B_6O material as function of temperature, respectively. Calculated thermal conductivities on the basis of these values for different temperatures are given in Table 4. Additionally the determined Coefficient of Thermal Expansion (CTE) and room temperature conductivities obtained by the direct measurement method are listed.

For all investigated materials the thermal diffusivity shows an exponential decay with increasing temperature. At room temperature values between 6.4 mm^2/s (sample nr-1) and 9.1 mm^2/s (pure material) are obtained while high temperature diffusivities at 1000 °C are in the range of 2.4 mm^2/s (pure material) and 3.4 mm^2/s (sample nr-2). Therefore highest room temperature diffusivities but also strongest decrease with increasing temperature is observed for the pure B_6O material. The addition of TiB_2 generally decreases thermal diffusivities although it is obvious that the non-reactive material with higher total TiB_2 amount (sample nr-2) is characterized by a higher thermal diffusivity in comparison to the sample with lower TiB_2 content (sample nr-1). Only small differences between the non-reactive and the reactive material with same composition (sample nr-1; r-1) are visible. The reactive material shows slightly higher thermal diffusivities at temperatures below 700 °C in comparison to its non-reactive counterpart with similar composition. The resulting calculated thermal conductivities are between 15 W/mK (sample nr-1) and 19 W/mK (pure material) at room temperature and in the range of 12 W/mK (pure material) and 18 W/mK (sample nr-2) at 1000 °C (Table 4). The calculated values at room temperature are in good agreement with the results obtained by the direct measurements of thermal conductivity near room temperature. For the pure material a thermal conductivity of 18.1 W/mK and for non-reactive sintered sample with 19.6 vol.% TiB_2 (sample nr-1) a value of 15.6 W/mK was measured.

The thermal expansion up to 1000 °C is characterized by a CTE of 5.65×10^{-6}/K for the pure material. The addition of 19.6 vol.% TiB_2 (sample nr-1) and 36.1 vol.% TiB_2 (sample nr-2) in non-reactive sintering gradually increases the thermal expansion to 6.22×10^{-6}/K and 6.63×10^{-6}/K, respectively. Reactive sintered material with 19.5 vol.% TiB_2 (sample r-1) is characterized by a slightly increased CTE of 6.58×10^{-6}/K

Table 4
Measured and calculated thermal conductivity and thermal expansion coefficient (CTE) for pure B_6O and B_6O/TiB_2 composites at different temperatures.

Sample	Measured $\lambda(T)$ (W/mK)	Calculated thermal conductivity $\lambda(T)$ (W/mK)				CTE $\alpha(T)$ ($\times 10^{-6}$/K)	
	RT	RT	400 °C	800 °C	1000 °C	800 °C	1000 °C
Pure	18.1 ± 0.9	19	17	14	12	5.46	5.65
nr-1	15.6 ± 0.9	15	17	15	14	6.02	6.22
nr-2	–	18	20	19	18	6.35	6.63
r-1	–	17	18	15	14	6.23	6.58

in comparison to the non-reactive sintered sample with similar composition.

4. Discussion

4.1. Densification and phase formation

4.1.1. Non-reactive

The densification of B_6O materials is complicated by low diffusion rates due to strong covalent bonding which cannot be easily compensated by the application of high temperature as boron compounds in general are characterized by a high vapor pressure. Therefore the use of sintering additives which form a liquid phase by reaction with B_2O_3 present on the surface of B_6O is reported to be a promising way to enhance densification of B_6O materials.[14–21]

As already shown by Herrmann et al. the addition of TiB_2 and oxide additives significantly enhances sintering and allows reproducible production of full densified samples.[14] This is more an effect of Al_2O_3/Y_2O_3 than TiB_2 addition. However, the investigations show that also the use of TiB_2 without additional sintering additives supports densification and allows reproducible production of dense materials at reasonable temperatures of about 1850 °C. TiB_2 is characterized by a very high melting point of about 3225 °C and requires itself high sintering temperatures above 2000 °C for densification.[22] Consequently, from sintering theory the densification of B_6O should therefore not be significantly enhanced by the addition of TiB_2 as only additive. At least an increased green density due to an increased grain size distribution could result upon admixing B_6O with TiB_2. Hence, considering the typical formation of an oxide layer of TiO_2 and B_2O_3 on the TiB_2 surface,[25] the improved densification may be mainly contributed to the formation of a liquid with additional B_2O_3 from the B_6O surface which can already take place at temperatures as low as 450 °C.[3] Therefore the densification of B_6O/TiB_2 composites may in principal be considered as a liquid phase assisted process. A further component of the liquid will be WO_3 which originates from the oxide layer on the introduced WC particles in the case of sample preparation by WC milling. WC itself will decompose under the release of carbon monoxide. This can be assumed since no carbon containing phases are present in the final materials. Probably this will occur by reaction with the liquid phase and thus the liquid will get further enriched in tungsten and depletion in oxygen will take place or B_2O_3 is partially reduced to B_6O. Coincidently, during the solution-precipitation stage a (Ti,W)B_2 solid solution is precipitated which epitaxially growth on the TiB_2 particles and will result in the observed core-rim structure of the TiB_2 grains. For this further TiB_2 has to be dissolved into the liquid. That this dissolution of TiB_2 takes place is also indicated by the observation of a rounded morphology of the TiB_2 core. Taken together the occurring reactions may be schematically summarized by following equitation:

$$(TiO_2 - B_2O_3 - WO_3)(l) + WC + B_6O + TiB_2 = (Ti, W)B_2 + CO(g) \quad (2)$$

However, it has to be mentioned that the decomposition of the WC was not investigated in detail. Because of only small differences of atomic radii for tungsten and titanium the (Ti,W)B_2 solid solution is characterized by nearly identical lattice parameters[27] and thus no separate phases could be assigned in XRD analysis. The tungsten content of the formed (Ti,W)B_2 was not quantified but from literature it is known that about 9 at% tungsten can be incorporated in the TiB_2 structure at 1850 °C.[27,28] The origin of measured minor amounts of Al in (Ti,W)B_2 can be attributed to a contamination in the synthesized B_6O powder. Although no continuous solid solution is observed between TiB_2 and AlB_2 limited integration is allowed by the structure.[29]

4.1.2. Reactive

In addition to prior investigations of Herrmann et al.[14] XRD and DTA/TG analysis of this work shows that the formation of B_6O and TiB_2 during the reactive sintering of B–TiO_2 mixtures takes place in separated steps. Initially an oxygen deficient compound TiO_{2-x} and $TiBO_3$ is partially formed at $T < 780$ °C from the initial B-TiO_2 mixture as seen in the XRD measurements (Fig. 3). This process probably corresponds to the weak exothermic effect below 600 °C in DTA measurement. This mixture is then finally converted to TiB_2 and B_2O_3 (liquid) at about 775 °C which corresponds to the observed strong exothermic effect. Assuming an average oxygen composition for the reduced TiO_{2-x} compound of Ti_2O_3, the reactions can be schematically expressed according to following equations:

$$B + 3TiO_2 = Ti_2O_3 + TiBO_3 \quad (3a)$$

$$Ti_2O_3 + TiBO_3 + 9B = 3TiB_2 + 2B_2O_3(l) \quad (3b)$$

From literature it is known that the formation of Ti_2O_3 and $TiBO_3$ by the reduction of titanium oxide with boron already occurs at temperature below 600 °C while TiB_2 formation takes place in a broad range of 700–1300 °C.[30,31] The following

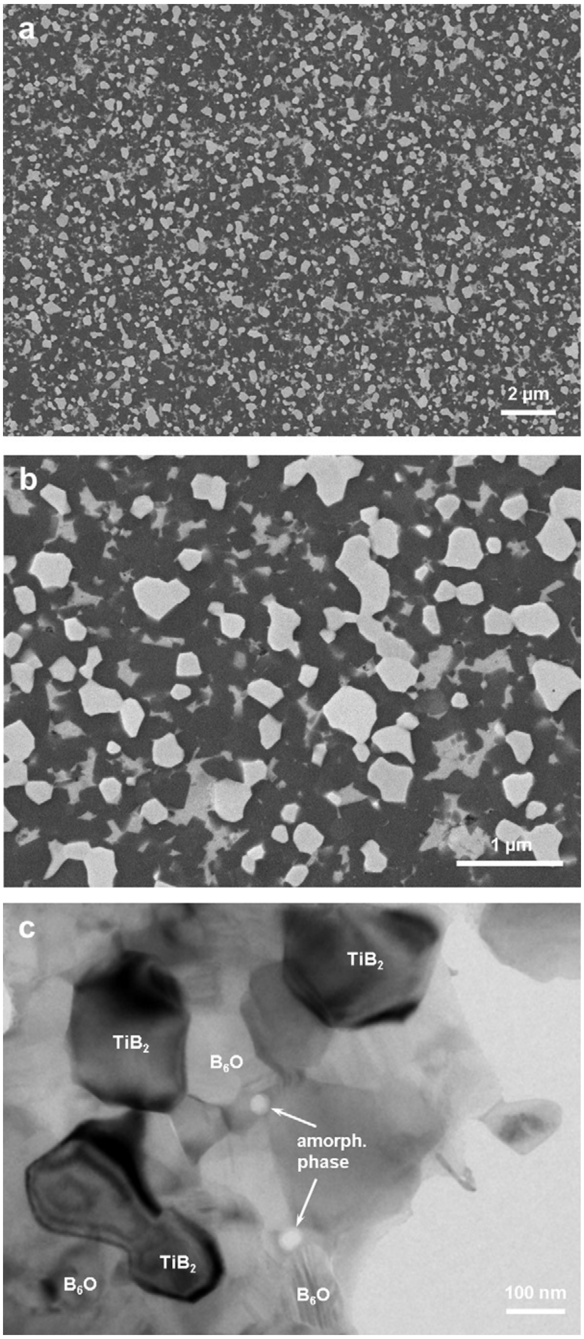

Fig. 6. Micrographs of reactive sintered materials: (a) SE-image of sample r-3a showing homogeneously distributed TiB_2 grains (bright) and irregular shaped oxide additives (less bright phase) in a matrix of B_6O (dark). (b) Higher magnification of (a) showing often well facetted TiB_2 grains. (c) TEM image of sample r-5ae with marked phases. Stacking faults in B_6O and phase separation in the amorphous Al–Y–O–B phase are visible (bright circular regions).

formation of B_6O could be assigned to the additional exothermic reaction at 1395 °C where the formed B_2O_3 reacts with the remaining boron according to the reaction:

$$16B + B_2O_3 = 3B_6O \tag{4}$$

This temperature is in agreement to the synthesis temperature of B_6O from mixtures of B and B_2O_3. However, it could not be excluded that already in reaction 3b amorphous B_6O is formed

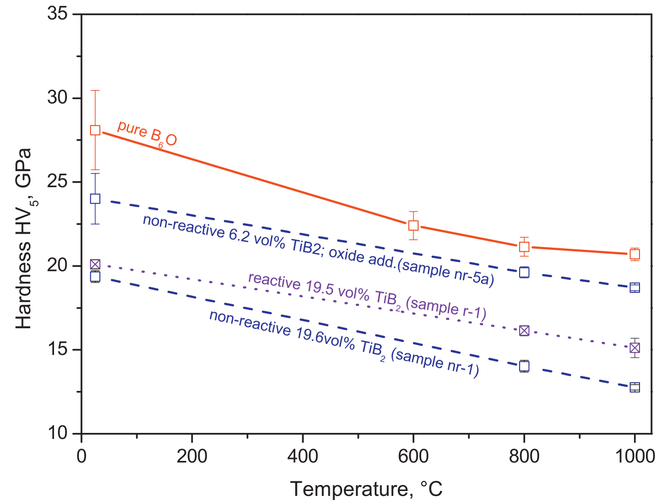

Fig. 7. Hardness HV_5 as function of temperature for reactive and non-reactive sintered B_6O/TiB_2 materials in comparison to a pure B_6O material.

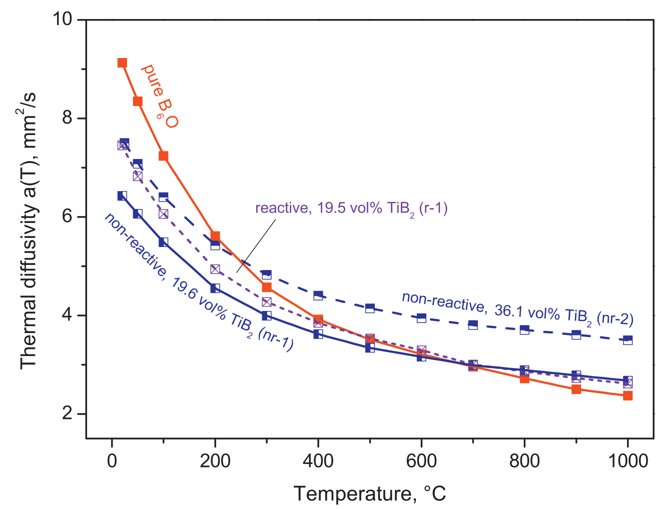

Fig. 8. Thermal diffusivity $a(T)$ as function of temperature for two non-reactive and a reactive sintered material in comparison to pure B_6O.

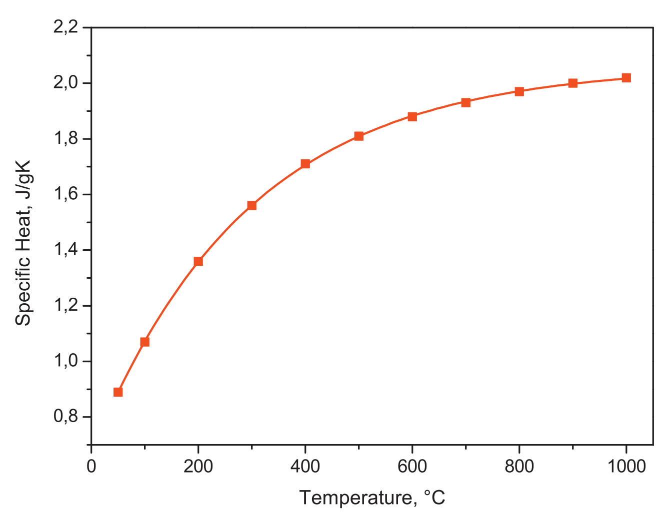

Fig. 9. Specific heat as function of temperature for sintered pure B_6O.

instead of B_2O_3. The exothermic effect at 1395 °C will then be connected with the crystallization of B_6O from its amorphous matter.

Correlating the observations with the recorded densification curves in Fig. 1 it is obvious that a considerable portion of densification is attributed to the first borothermic reaction step. Moreover, it is also visible that strong densification continuous up to a temperature of about 1400 °C. In respect to the XRD results this may be contributed to the low crystallinity of the early formed TiB_2 since a high defect concentration can drastically improve the sintering kinetics which was shown already for comparable materials with low sinterability.[33,34] Finally at 1400 °C a relative density of about 70% is achieved, while non-reactive densification procedure provides 15–20% lower densities at the same temperature. XRD measurement of the reactive sample at 1470 °C reveals a lower crystallinity of the B_6O in comparison to the fully densified samples. Consequently, a sintering temperature up to 1800–1850 °C is required for obtaining a well crystallized and dense material in the used sintering regime.

Similar to the non-reactive synthesis route it could be shown that the addition of oxide additives to a reactive TiO_2-B mixture does not notably interfere with the starting materials and also lead to the formation of an amorphous additive phase. Since densification is dominated by TiB_2 and B_6O formation no clear indication for the enhancement of sintering by the use of oxide additives were observed neither in densification curves nor in the resulting densities.

In this work calculations of the initial B/TiO_2 ratio for reactive sintered compositions were done using reaction 1, assuming the formation of stoichiometric B_6O. However, it is widely accepted that B_6O synthesis at low pressure results in formation of oxygen deficient compositions.[35–40] Thus, considering the formation of a reasonable substoichiometric composition of about $B_6O_{0.8}$[40] at the sintering conditions, the reactive sintered materials (samples r-1; r-3a; r-4a) should be composed of some additional B_2O_3 or TiO_2. This was not observed in microstructure analysis. However, it is not clear whether B_2O_3 has formed or not since it could not be easily located in microstructure investigations because it is leeched out during sample preparation and also highly electron-beam sensitive. In the case of alumina and yttria additives used, B_2O_3 will also contribute to the formation of the amorphous phase. Alternatively, the missing B_2O_3/TiO_2 can be easily explained taking the evaporation of some B–O compounds during sintering into account. The observed mass loss during DTA/TG analysis in Fig. 2 would be in the range of the required amount for obtaining the estimated stoichiometry of $B_6O_{0.8}$ (approximately 3 wt.% loss expected if $B_6O_{0.8}$ is formed). For the reduction of oxygen stoichiometry by adding 12 wt.% boron in excess the formation of additional boron in the final material was observed (samples r-2e; r-5ae). As an excess of 12 wt.% boron means a hypothetical formation of $B_6O_{0.78}$ in reaction 1 one may conclude that the formed B_6O is therefore at least characterized by a higher stoichiometry. An influence of additional boron on densification is not observed.

In comparison to the non-reactive sintering route, the reactive sintering of B–TiO_2 mixtures according to Eq. (1) provides a significant improvement of densification and reduces production costs due to unnecessary prior synthesis of B_6O and TiB_2 powder. Additionally, in terms of the densification process another advantage is a decreased grain growth beside the reduction of interaction with the sintering equipment and furnace atmosphere due to more intense densification at lower temperatures. However, in this work the same sintering regime was used for all produced B_6O/TiB_2 composites regardless of the preparation route. It is likely that the optimization of the sintering regime for the reactive compositions, i.e. by an additional dwelling time during the strong densification at $T < 1400$ °C, may significantly enhance the densification and thus allow the production of full densified B_6O/TiB_2 composites at lower total temperatures. To some extent it was exemplary tried to apply the mechanical load during sintering already at temperatures below 800 °C before first strong densification in reactive sintered materials takes place. However, no effect on the overall densification behavior was observed.

4.2. *Microstructure and properties*

4.2.1. *Hardness*

Similar to many other ultra- and superhard materials, the hardness of B_6O materials is affected by the indention size effect (ISE) which results in load depending hardness values and the absence of a single hardness values.[21,41] The obtained hardness which is given in Table 3 shows that the microhardness at a load of 3.9 N is generally about 30% higher than the values obtained for a testing load of 49 N. Moreover the correlation of the hardness with compositional and microstructural properties is not straight forward since the measured values of macrohardness HV_5 and microhardness $HV_{0.4}$ are not always consistent to each other and often do not follow the same trend. This is especially observed for very high hardness values as resulting for reactive sintered samples. For instance, the sample r-4a is characterized by the highest measured microhardness (36 GPa) of all composite materials but contrary shows also the lowest macrohardness (22 GPa) of all reactive sintered compositions. Another example is the reactive sintered material r-2e which is characterized by the highest macrohardness (28 GPa) of all composite materials but has only moderate microhardness (32 GPa). In the non-reactive materials these discrepancies are not that obvious because of higher compositional differences and therefore a broader range of hardness values. These inconsistencies can mainly be attributed to the general difficulties of a reproducible measurement of high hardness by indention method. Furthermore and although the obtained standard deviations of measured hardness values are fairly small, hardness measurements cover only a small sample area and are therefore sensitive to local variances of sample composition and porosity.

Apart from that it is observed that the non-reactive as well as the reactive compositions without oxide additives are preferentially affected of TiB_2 phase pullouts during mechanical sample preparation. This introduced porosity may significantly affect the measured hardness. This is thought to be the reason for the low hardness of the reactive sintered material r-1. Although no clear proofs for a weakened interface in samples without oxide additives were found in TEM investigation, TiB_2 grain pullouts

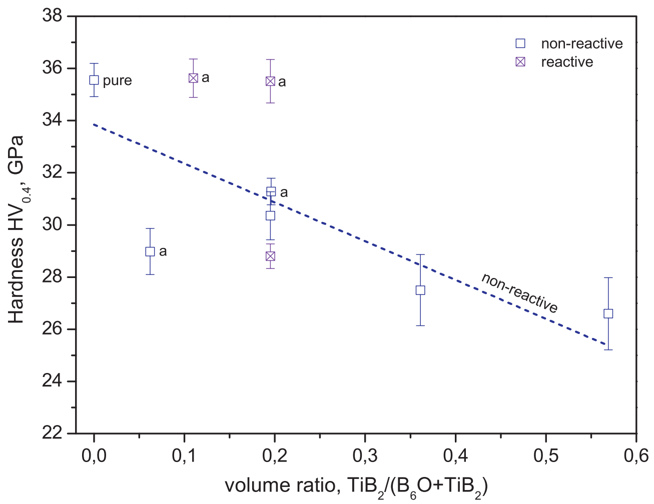

Fig. 10. Microhardness as function of $TiB_2/(B_6O + TiB_2)$ volume ratio for non-reactive and stoichiometric reactive compositions (without excess boron). Compositions with additional oxides are marked with an "a". A linear function on the basis of the data for non-reactive materials including the pure material is plotted.

are probably caused by differences in the CTE between TiB_2 and the surrounding matrix. Considering a thermal expansion of 5.65×10^{-6}/K for the pure B_6O material (this work) or 5.5×10^{-6}/K,[42] respectively, and about 6.2×10^{-6}/K[43] for a B_6O material with oxide additives, the thermal expansion mismatch between TiB_2 (8.6×10^{-6}/K [22]) and the matrix will be significantly larger in the case that no oxide additives are used and thus resulting in weakened B_6O/TiB_2 interfaces and phase pullout due to arising tensile stresses.

However, keeping these uncertainties in hardness measurements in mind, the investigations clearly show that the reactive sintering path produces B_6O/TiB_2 materials with significant higher hardness than that resulting from the non-reactive route which is mainly connected with a much finer microstructure. Hardness in reactive sintering route approaches that of pure B_6O. Therefore the small grain size of the reactive sintered materials compensates the general decrease of hardness due to the incorporation of lower hardness phase in the B_6O matrix. Fig. 10 illustrates the measured hardness as function of TiB_2 content for non-reactive as well as reactive samples with stoichiometric composition (without boron in excess). The broad variation of TiB_2 amount in the non-reactive samples shows a fairly linear trend of decreasing hardness with increasing TiB_2 content. It is also obvious that the non-reactive sample with the lowest TiB_2 amount and oxide additives (sample nr-5a) show an unexpected low microhardness which does not fit to the trend. Moreover, Herrmann et al. reported a microhardness $HV_{0.4}$ of 36.8 ± 0.6 GPa for a sample with nearly equal composition (10 wt.% TiB_2, 4 wt.% oxide additives), density and preparation procedure.[14] Therefore the reason for the low microhardness value is not clearly understood. At least the macrohardness HV_5 of this sample indicates that the measured microhardness of this sample may be much lower than expected. However, the value was confirmed in a second measurement which resulted in an even lower microhardness of 27.3 ± 0.9 GPa. Therefore, further investigations are necessary.

In respect to the measurement uncertainties and the phase-pullout-effect no direct influence of the oxide additive addition in non-reactive as well as reactive compositions could be observed on the measured hardness even tough about 10 vol.% of an amorphous phase is formed upon addition of 4.4–4.8 wt.% oxides. This is in agreement with recently reported observations which point out that the hardness of B_6O materials is only marginally affected by the addition of small amounts of Al_2O_3/Y_2O_3 additives.[14,15,21,43] The presence of some non-reacted boron in the microstructure of the reactive compositions with boron in excess results in a slightly reduced hardness. Especially sample r-2e is characterized by a relative high scattering of the macrohardness suggesting local inhomogeneities by the presence of the weaker boron phase.

4.2.2. High temperature hardness

The relative decrease of hardness with increasing temperature is nearly similar for all composite materials. The high temperature hardness therefore reflects the trend of room temperature hardness where the hardness decreases with increasing TiB_2 amount. At least, the grain size effect which causes a higher hardness of reactive materials in comparison to its non-reactive counterpart with similar composition shows the tendency to become even larger with rising temperature. Comparing the obtained results with high temperature hardness values of oxide additive including B_6O materials reported earlier,[21,43] it can be concluded that the addition of low TiB_2 amounts results in a significant higher hardness at 1000 °C for the non-reactive composition with low amounts of TiB_2 including oxide additives (20 GPa) in comparison to the sample with oxide additives only (17 GPa). The high temperature hardness values of sample nr-5a is also significantly higher than that obtained for commercial c-BN (15.5 ± 0.4 GPa)[21,43] and reaches the values obtained for commercial B_4C at 1000 °C (20.0 ± 0.7 GPa).[21] Even the reactive sample with 19.5 vol.% TiB_2 (sample r-1) shows a high temperature hardness comparable to that of commercial c-BN materials.

4.2.3. Fracture toughness

A main motivation for this work was the investigation whether the fracture toughness of B_6O materials can be improved by forming composite materials with TiB_2 and thus one of the main shortcomings towards commercial application of B_6O materials can be reduced or eliminated. Both, the results of the measurement by the IF method as well as the more reliable values obtained in SEVNB method indicate that the fracture toughness is significantly improved in all produced B_6O materials by the addition of TiB_2 (Fig. 11). Because of the broad variation of the TiB_2 amount in the non-reactive materials, it can be clearly seen that the fracture toughness is linearly increasing with rising TiB_2 content to values up to 5 MPa $m^{1/2}$ for the highest $TiB_2/(B_6O + TiB_2)$ volume ratio of about 0.6. In respect to an estimated relative error of 15–20% for the fracture toughness obtained by the IF method the measured values reveal no distinct indications of the role of oxide additives and whether the reactive or non-reactive route provide more fracture resistant materials. However, especially for the reactive

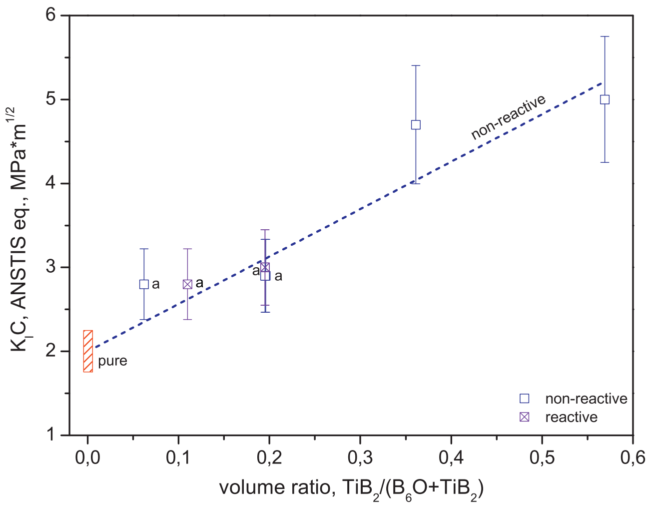

Fig. 11. Fracture toughness (IF method, Anstis equitation) as a function of $TiB_2/(B_6O + TiB_2)$ volume ratio for the non-reactive as well as for the stoichiometric reactive compositions (without excess boron). Compositions with additional oxides are marked with an "a". The fracture toughness of the pure material is estimated. A linear function through the data of the non-reactive materials is plotted.

sintered materials simultaneously a very high microhardness is preserved due to their fine microstructure. SEVNB testing was only exemplary done and therefore no preference for specific sample compositions can be seen. Nevertheless in comparison to the pure material the obtained values show an improvement of fracture resistance in the range of 50–100% upon the addition of about 20 vol.% TiB_2 (and oxide additives). Thus the fracture toughness of the composite materials is in the range of B_6O materials with oxide additives only.[15,21]

The resulting fracture path near the crack tip for a non-reactive (sample nr-4a) as well as reactive sintered material (sample r-3a) with oxide additives, respectively, is illustrated in Fig. 12. Several crack deflection events on TiB_2 particles can be observed in both materials while crack propagation in the B_6O matrix is predominantly transgranular which was already observed in prior works.[15,17,21] Furthermore crack arresting on TiB_2/B_6O boundaries occurs. These mechanisms are a suitable explanation for the improved fracture toughness and are caused by the differences in the thermal expansion between the TiB_2 particles and the B_6O matrix. The larger CTE of TiB_2 (8.6×10^{-6}/K) in comparison to that of the B_6O matrix (5.65×10^{-6}/K) will form tensile stress at the TiB_2/B_6O grain boundaries and therefore result in the deflection or arresting of passing cracks. Although these toughening mechanisms are observed in reactive as well as in the non-reactive sintered compositions, it is conclusive that the increase of fracture resistance will be in principal higher in reactive sintered materials due to the finer microstructure and therefore more energy dissipative toughening events taking place. However, this could not be observed. Further reliable SEVNB measurements have to be performed.

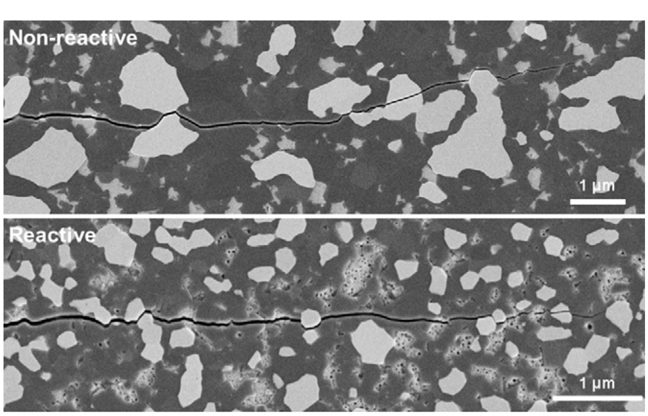

Fig. 12. SE-image of the crack path near the crack tip in non-reactive (top) and reactive (bottom) sintered B_6O/TiB_2 composite containing 19.5 vol.% TiB_2 and oxide additives, respectively (samples nr-4a; r-3a).

In contrast to the role of TiB_2 particles the amorphous additive phase seems only to contribute indirectly to the fracture resistance since crack propagation is predominantly transgranular. However, the prevention of the TiB_2 phase pullout during mechanical polishing indicate that the formation of an amorphous Al–Y–O–B phase may significantly decrease the residual stresses between the TiB_2 particles and the surrounding matrix and thus will also influence the resulting fracture toughness despite of the absence of common toughening mechanism like crack arresting, bridging or branching. Large residual stresses are known to additionally result in microcracking with partial or complete fracture of the interface which will also contribute to an improvement in fracture toughness. Although microcracks or weakened interfaces were not observed by TEM, investigations in the SiC–TiB_2 system with similar differences of the CTEs[44] suggesting that this mechanism may also be important for B_6O/TiB_2 composites. Another important but so far also speculative mechanism might be related to the role of twinning planes and stacking fault on the crack propagation. Although twins are planar defects, they have been reported to contribute to the fracture toughness in boron carbide[45] which is isostructural to B_6O. The fracture mode in B_6O materials is predominantly transgranular therefore the twins may inhibit crack propagation by acting as barrier, deflect the crack and force it to propagate along the subgrain boundaries. Taking this into account a higher fracture toughness would be expected for the materials prepared by the non-reactive preparation route since TEM investigation show that B_6O in non-reactive sintered materials exhibit a significant higher defect density than B_6O resulting from reactive sintering route. This is probably caused by the relative low sintering temperature of the starting B_6O powder for the non-reactive sintering route as well as a longer exposure to pressure during sintering. However due to the overlapping with other effects and measurement uncertainties this could not be seen in the measured values. Again further investigations are necessary to clarify the role of twinning and stacking faults on the mechanical behavior of B_6O/TiB_2 composites as well as B_6O materials.

4.2.4. Thermal conductivity

In cutting and wear applications it is essential to avoid excessive temperature gradients. Thus the thermal conductivity can be considered as a major key property of wear resistance materials. In agreement to thermal properties of a (porous) B_6O material reported by Bairamahvili et al., B_6O is generally characterized by a decreasing thermal conductivity with increasing temperature, which could be assigned to the dominating mechanism of heat transfer by phonons in the investigated temperature range.[42] The formation of B_6O/TiB_2 composites reduces the decrease of thermal conductivity with rising temperature and results in significant improved values in comparison to pure B_6O materials. The reason for that is a much higher intrinsic thermal conductivity of the TiB_2 phase which additionally only decreases about 20% in the range between room temperature and 1000 °C (RT: 96 W/mK, 1000 °C: 78.1 W/mK [22]). However, upon addition of TiB_2 into a B_6O matrix the thermal conductivity at room temperature is initially lowered. Although the calculated values are not conclusive, because of a relative large error of about 15% this effect can be clearly seen in the values exemplary obtained by the direct measurement near room temperature. A possible explanation for that would be a prevailing effect of an increased number of phase boundaries introduced in B_6O/TiB_2 composites which decrease the phonon mean-free path in comparison to a pure B_6O material. With increasing temperature this effect is compensated by the larger thermal conductivity of TiB_2 at high temperatures.

Data for the thermal conductivity of B_6O materials are rare in literature. Currently unpublished data of the authors for B_6O materials with oxide additives give a thermal conductivity of 12–18 W/mK which is decreased to 9–14 W/mK at 1000 °C. In comparison commercial cBN materials provide a thermal conductivity at room temperature of about 44–100 W/mK.[46]

5. Conclusions

Full densified B_6O/TiB_2 composites were produced by a non-reactive as well as a reactive preparation route using FAST/SPS at temperatures in the range of 1850–1900 °C. The sintering behavior, resulting microstructure and the mechanical and thermal properties were characterized and compared with that of a pure B_6O material.

It could be shown that the reactive sintering route on the basis of B–TiO_2 mixtures is characterized by an improved densification in comparison to the non-reactive preparation procedure and provides a cost-effective way for producing B_6O/TiB_2 composite without the necessity of prior B_6O and TiB_2 synthesis. B_6O and TiB_2 formation in reactive sintering occurs in mainly two separate reactions steps for TiB_2 and B_6O formation at temperatures of about 780 °C and 1400 °C, respectively. Also in the non-reactive route an improved densification in comparison to pure B_6O without sintering additives was observed upon adding of TiB_2.

Reactive sintering results in a much finer microstructure. Thus a higher hardness in the range of 29–36 GPa ($HV_{0.4}$) and 22–28 GPa (HV_5) is obtained for the reactive compositions in comparison to 27–31 GPa ($HV_{0.4}$) and 15–24 GPa (HV_5) for the non-reactive preparation procedure, respectively. Up to 1000 °C the macrohardness HV_5 reduces about 25–33%. The resulting high temperature hardness partially exceeds that of commercial c-BN tools and prior reported values for B_6O materials with oxide additives and is up to 20 GPa at 1000 °C.

The addition of TiB_2 in a matrix of B_6O significantly increases the fracture toughness. The main mechanisms for that are crack deflection and crack arresting on the introduced TiB_2 particles. For the non-reactive compositions the crack resistance is nearly linearly increased up to a total TiB_2 amount of about 60 vol.% where a fracture toughness of 5.0 MPa $m^{1/2}$ (IF method) is obtained. However, comparing materials with similar composition no definite differences in the fracture resistance between the non-reactive and the reactive preparation route could be resolved. Resulting values for all composite materials are in the range of 3.1–4.0 MPa $m^{1/2}$ (SEVNB).

A thermal conductivity at room temperature between 15 and 18 W/mK is measured which is slightly lower than that of pure B_6O, The characteristic drop of thermal conductivity with increasing temperature for pure B_6O materials is compensated by the addition of TiB_2. High temperature thermal conductivities at 1000 °C of 14–18 W/mK are obtained for the composites while higher values are retrieved for lower B_6O/TiB_2 ratios. The thermal expansion is in the range of $6.22–6.58 \times 10^{-6}$/K.

The use of oxide additives results in the formation of an additional amorphous phase in non-reactive as well as reactive compositions. It decreases the tensile stress between the TiB_2 particles and the B_6O matrix and therefore prevents a weakened interface and a resulting pullout of the TiB_2 phase.

Taken together, the study indicates that B_6O/TiB_2 composites (and especially the reactive sintering route) are a promising approach to improve the densification and the fracture toughness of B_6O materials which currently are the main obstacles towards commercial applications. An optimization of the sintering regime is necessary for taking full advantage of the improved densification behavior of the reactive compositions. In order to optimize the material properties more detailed investigations of the influence of the B_6O/TiB_2 ratio, the role of additives and the B_6O stoichiometry are necessary.

Acknowledgment

The authors acknowledge Element Six Ltd for the financial support of the research.

References

1. He D, Zhao Y, Daemen L, Qian J, Shen TD, Zerda TW. Boron suboxide: as hard as cubic boron nitride. *Appl Phys Lett* 2002;**81**(4):643–5.
2. Olofsson M, Lundstroem T. Synthesis and structure of non-stoichiometric B_6O. *J Alloys Compd* 1997;**257**:91–5.
3. Holcombe Jr CE, Horne Jr OJ. Preparation of boron suboxide, B_7O. *J Am Ceram Soc* 1972;**55**:106.
4. Kuo SY, Csillag FJ, Zandi M, Hayashi CEH. Boron Suboxide Material and Method for its Preparation, US Patent 5,135,892; 1992.
5. Lundstroem T. Structure and bulk modulus of high-strength boron compounds. *J Solid State Chem* 1997;**133**:88–92.
6. Hubert H, Garvie LAJ, Devouard B, Buseck PR, Petuskey WT, McMillan PF. High-pressure, high-temperature synthesis and characterization of boron suboxide (B_6O). *Chem Mater* 1998;**10**:1530–7.
7. Hubert H, Garvie LAJ, Devouard B, McMillan PF. High-pressure, high-temperature syntheses of super-hard alpha-rhombohedral boron-rich solids in the B–C–N–O. *Mater Res Soc Symp Proc* 1998;**499**:315.
8. Itoh H, Maekawa I, Iwahara H. High pressure sintering of B_6O powder and properties of sintered compact. *J Soc Mat Sci Japn* 1998;**47**:1000–5.

9. Sasai R, Fukatsu H, Kojima T, Itoh H. High pressure consolidation of B_6O–diamond mixtures. *J Mater Sci* 2001;**36**:5339–43.
10. Itoh H, Maekawa I, Iwahara H. Microstructure and mechanical properties of B_6O-B_4C sintered composites prepared under high pressure. *J Mater Sci* 2000;**35**:693–8.
11. Itoh H, Yamamoto R. B_6O-cBN composites prepared by high-pressure sintering. *J Am Ceram Soc* 2000;**83**:501–6.
12. Ellison-Hayashi C, Zandi M, Shetty DK, Kuo P, Yeckley R, Csillag F. Boron suboxide material and method for its preparation, US Patent 5,135,895; 1992.
13. Goosey BF, Anderson SC, Method of fabricating boron suboxide articles, US Patent 3,816,586; 1974.
14. Herrmann M, Raethel J, Bales A, Sempf K, Sigalas IJ, Hoehn M. Liquid phase assisted densification of superhard B_6O-materials. *J Eur Ceram Soc* 2009;**29**:2611–7.
15. Herrmann M, Kleebe H-J, Raethel J, Sempf K, Lauterbach S, Müller MM, et al. Field-assisted densification of superhard B_6O materials with Y_2O_3/Al_2O_3 addition. *J Am Ceram Soc* 2009;**92**:2368–72.
16. Andrews A, Herrmann M, Shabalala TC, Sigalas I. Liquid phase assisted hot pressing of boron suboxide materials. *J Eur Ceram Soc* 2008;**28**:1613–21.
17. Kleebe H-J, Lauterbach S, Shabalala TC, Herrmann M, Sigalas IJ. B_6O: a correlation between mechanical properties and microstructure evolution upon Al_2O_3 addition during hot-pressing. *J Am Ceram Soc* 2008;**91**(2):569–75.
18. Johnson OT, Sigalas I, Ogunmuyiwa EN, Kleebe HJ, Mueller M, Herrmann M. Boron suboxide materials with Co sintering additives. *Ceram Int* 2010;**36**:1767–71.
19. Johnson OT, Sigalas I, Herrmann M. Microstructure and interfacial reactions between B_6O and (Ni, Co) couples. *Ceram Int* 2010;**36**:2401–6.
20. Shabalala TC, McLachlan DS, Sigalas II, Herrmann MM. Hard and tough boron suboxide based composites. *Ceram Int* 2008;**34**:1713–7.
21. Thiele M, Herrmann M. Boron suboxide with oxide additives for cutting and wear applications. In: *12th Conference of the European Ceramic Society*. 2011.
22. Munro RG. Material properties of titanium diboride. *J Res Natl Inst Stand Technol* 2000;**105**:709–20.
23. Mendelson MI. Average grain size in polycrystalline ceramics. *J Am Ceram Soc* 1969;**52**:443–6.
24. Anstis GR, Lawn BR, Marshall DB, Chantikul P. A critical evaluation of indentation techniques for measuring fracture toughness: I, Direct crack measurements. *J Am Ceram Soc* 1981;**64**:533–8.
25. Park J-H, Lee Y-H, Koh Y-H, Kim H-E, Su Baek S. Effect of hot-pressing temperature on densification and mechanical properties of titanium diboride with silicon nitride as a sintering aid. *J Am Ceram Soc* 2000;**83**:1542–4.
26. FACTSAGE 5.5, SGPS database (January 2007)—SGTE pure substance database, A.T., Dinsdale, SGTE Data for Pure Elements, CALPHAD, 15(4), 1991, 317–425.
27. Mitra I, Telle R. Phase formation during anneal of supersaturated TiB_2–CrB_2–WB_2 solid solutions. *J Solid State Chem* 1997;**133**:25–30.
28. Telle R, Fendler E, Petzow G. The quasi-binary systems CrB_2–TiB_2, CrB_2–WB_2 and TiB_2–WB_2. *J Hard Mater* 1992;**3**:211–24.
29. Raghavan V. Al–B–Ti (Aluminum–Boron–Titanium). *J Phs Eqil and Diff* 2005;**26**(2):173–4.
30. Jiang Z, Rhine WE. Preparation of titanium diboride from the borothermic reduction of TiO_2, $TiO_x(OH)_y$ or $Ti(O–n–Bu)_4$-derived polymers,. *J Eur Ceram Soc* 1993;**12**:403–11.
31. Millet P, Hwang T. Preparation of TiB_2 and ZrB_2 influence of a mechanochemical treatment on the borothermic reduction of titania and zirconia. *J Mater Sci* 1996;**31**:351–5.
33. Rodriguez VZ, Galán CA, Cabanillas FG, Shaw LL, Nygren M. Towards the sintering of ultra-high-temperature ceramics at lower temperatures. In: *12th Conference of the European Ceramic Society*. 2011.
34. Rodriguez VZ, Seco ALO, Cabanillas FG, Nygren M. Effect of high-energy ball-milling on the spark-plasma-sintering kinetics of additive-free ZrB_2. In: *12th Conference of the European Ceramic Society*. 2011.
35. Brodhag C, Thévenot CF. Hot pressing of boron suboxide $B_{12}O_2$. *J Less-Common Met* 1986;**110**:1–6.
36. Bolmgren H, Lundström T, Okada S. Structure refinement of the boron suboxide (B_6O) by the Rietveld method. *AIP Conf Proc* 1991;**231**: 197.
37. Ellison-Hayashi C, Zandi M, Murray M, Csillag FJ, Kuo S. Boron suboxide material and method for its preparation, US Patent 5,135,895; 1992.
38. Kobayashi M, Higashi I, Brodhag C, Thevenot F. Structure of B_6O boron suboxide by Rietveld refinement. *J Mater Sci* 1993;**28**:2129.
39. Lundstrom T, Andreev YG. Superhard boron-rich borides and studies of the B–C–N system. *Mater Sci Eng A Struct* 1996;**209**:16.
40. Olofsson M, Lundström T. Synthesis and structure of non-stoichiometric B_6O. *J Alloys Compd* 1997;**257**:91.
41. Machaka R, Derry TE, Sigalas I. Nanoindentation hardness of hot-pressed boron suboxide. *Mater Sci Eng A* 2011;**528**:5778.
42. Bairamashvili IA, Kalandadze GI, Eristavi AM, Jobava JS, Chotulidi VV, Saloev Y. An investigation of the physicomechanical properties of boron oxide (B_6O) and silicon tetraboride. *J Less-Common Met* 1979;**67**:455.
43. Herrmann M, Swarnakar A, Thiele M, van der Biest O, Sigalas I. High temperature properties of B_6O-materials. *J Eur Ceram Soc* 2011.
44. Steinbrech RW. Toughening mechanisms for ceramic materials. *J Eur Ceram Soc* 1992;**10**:131–42.
45. Oleinik G, Ostapchuk T. Effect of pores on the cleavage of twinned boron carbide crystals. *Powder Metall Metal Ceram* 1996;**34**:500.
46. Davis R, editor. *ASM specialty handbook, tool materials*. Materials Park, OH: ASM, International; 1995.